RESEARCH ARTICLE

Multi-Point RCNN for Predicting Deformation in Deep Excavation Pit Surrounding Soil Mass

FEI SONG[1], HUIWU ZHONG[2], JIAQING LI[3], AND HUAYONG ZHANG[1]

[1]Huanan Construction Company Ltd., China Construction Sixth Engineering Bureau, Shenzhen 518000, China
[2]Guangdong Shengxiang Traffic Engineering Testing Company Ltd., Guangzhou 511400, China
[3]Guangdong Highway Engineering Quality Supervision and Inspection Center, Guangzhou 510500, China

Corresponding author: Jiaqing Li (jiaqing_li_work@126.com)

ABSTRACT Accurate prediction and forecasting of soil mass deformation in deep excavation pits are pivotal for risk monitoring and safety assessment. Nonetheless, the complex underlying dynamics inherent in field sensing measurements pose challenges to the forecasting endeavor. In light of these challenges, the present study leverages recent strides in deep learning and introduces a spatiotemporal learning framework tailored to forecast soil mass deformation marked by resilient temporal interconnections and spatial associations. This study focuses on developing a Multi-Point Recurrent Convolutional Neural Network (RCNN) model for predicting sensor-based temporal patterns. This model integrates data feature fusion to extract spatiotemporal latent features from the dataset, thereby constructing a surrogate model for forecasting soil mass deformation. The proposed methodology is deployed to forecast strain responses in a deep excavation pit using a dataset spanning over five months. A comparative analysis is conducted, contrasting the performance of the proposed approach with that of a conventional temporal-only network. The analysis reveals that the prediction errors generated by the Multi-Point RCNN are predominantly concentrated within the range of 10% for all sensors, with a high-confidence interval (CI) of 96%, compared to the RCNN model (82%) and the LSTM model (79%). The compelling outcomes underscore the efficacy of the Multi-Point RCNN approach as a promising, dependable, and computationally efficient method for accurately predicting soil mass deformation in deep excavation pits, grounded in data-driven principles.

INDEX TERMS Deep excavation pits, predicting deformation of soil mass, deep learning, multi-point RCNN.

I. INTRODUCTION

Excavation endeavors within foundation pit projects encompass a myriad of influential factors, imparting noteworthy challenges to the construction process. As the scale of excavation expands, the associated engineering risks exhibit a marked escalation [1], [2]. The soil situated within the pit undergoes transformations in both internal and external pressures, attributed to the unloading induced by excavation. These transformations engender modifications in the internal forces acting upon the support structure, consequently giving rise to displacement and deformation. Inadequate structural strength or stiffness can engender the inclination of support piles, occurrences of soil collapse, and substantial repercussions, such as floor fractures, pipeline impairment, and uneven settling of adjacent edifices [3], [4]. In this context, the implementation of dynamic monitoring during foundation pit excavation assumes particular significance. By promptly adapting construction processes and support parameters guided by monitoring data, the realization of information-centric construction becomes attainable. This approach ensures that the foundation pit is established in a manner that prioritizes safety and cost-effectiveness.

Deformation resulting from excavation within foundation pits is subject to a range of influencing factors, including geological parameters and construction methodologies [5], [6]. The intricacies of the actual deformation mechanism far surpass theoretical assumptions, and the intricate geological conditions introduce an element of

The associate editor coordinating the review of this manuscript and approving it for publication was Tao Zhou.

variability in the geomechanical properties of strata that defy absoluteness [7]. As a result, the precise prediction of lateral deformation in retaining structures during excavation processes has consistently posed a formidable challenge. In conventional foundation pit research, techniques such as finite element software modeling frequently serve as tools for deformation analysis [8], [9], [10]. Nonetheless, these approaches come with inherent limitations. Notably, the mechanical attributes of strata in finite element models often necessitate some level of simplification. Furthermore, the constitutive models employed for materials might inadequately capture the stress-strain relationships observable in engineering practice [11]. Actual construction processes also tend to be more intricate than the construction scenarios simulated in numerical models [11]. Hence, in many instances, finite element models struggle to comprehensively and authentically depict the excavation conditions of foundation pits. Adding to the challenge, the deformation outcomes derived from finite element models primarily correspond to data spanning extended time intervals or generalized construction phases [12]. This hinders the precise determination of foundation pit deformation on a daily basis, thus rendering accurate acquisition of deformation data for forthcoming days unattainable. Consequently, the practical utility of deformation control in engineering applications remains constrained.

In recent times, propelled by the progress in computer processing capabilities, emerging technologies such as neural network models and intelligent algorithms have undergone swift advancements [13], [14], [15], [16], [17], [18]. The Long Short-Term Memory (LSTM), originally conceived by two computer scientists [19], represents an intelligent algorithm that manifests distinct advantages in managing nonlinear data and time series. Its prowess lies in the prediction of time series data, surpassing conventional methods like Backpropagation (BP) neural networks, particularly in the domain of deformation prediction. The myriad influences impacting foundation pit deformation find essential expression in historical deformation data. The discerning memory modules inherent to the LSTM algorithm facilitate the consideration of the historical data's impact on the present state [20]. Through the discernment of inherent patterns within the temporal progression of extant deformation data, LSTM has the capacity to deduce abstract weight sets and mapping relations, rendering it apt for prognosticating deformation within foundation pit excavation.

Xie et al. [21] conducted an investigation pertaining to steep slopes in the southwestern region of China. They devised a dynamic prediction model based on LSTM to prognosticate landslide displacement. The findings underscored the superior dynamic attributes of the LSTM prediction model in comparison to conventional mechanical models. Zhang et al. [22], in a separate study, developed an LSTM model to anticipate maximum surface settlement and longitudinal settlement curves generated by tunnel boring machine excavation. The outcomes underscored the robustness of the

LSTM model, underscoring its adaptability across diverse classifications of subterranean engineering. In another vein, Qian et al. [23] formulated an LSTM combined prediction model tailored for the anticipation of surface settlement prompted by foundation pit excavation. The research illuminated that under stable working conditions, the LSTM model exhibited relatively modest predictive discrepancies. Moving forward, Zhao et al. [24] focused on a subway foundation pit project located in Suzhou. They harnessed both Backpropagation (BP) neural networks and LSTM intelligent algorithms to fabricate prediction models for lateral deformation within subterranean retaining walls. The predictive stability of these models was duly verified. The outcomes elucidated that the LSTM model attained heightened predictive precision when contrasted with conventional neural network models.

The previously mentioned studies primarily centered on utilizing single-point monitoring data as input and employed LSTM modeling for individual data point predictions. However, the deformation encompassing the excavation structure and the contiguous soil mass isn't isolated; instead, a certain interdependency exists among adjacent deformation entities. The methodology of separate prediction for each distinct point, followed by statistical modeling of the outcomes, frequently results in substantial disparities between the prognostications and the factual engineering circumstances. Consequently, the present investigation adopts an innovative approach. In order to forecast the deformation resulting from foundation pit excavation, a multi-point prediction model is adopted, encompassing the integration of data feature fusion. This model exhibits the aptitude to meticulously encapsulate the interrelationships between the envisaged deformation entity and the neighboring deformation entities. Within this context, a predictive framework is devised for projecting the deformation occurring in the surrounding soil mass within foundation pits. This framework is established on the foundational tenets of a Multi-Point Recurrent Convolutional Neural Network (RCNN).

II. PROBLEM STATEMENT

The process of deep excavation structure evolution spans an extended duration from construction inception to potential failure occurrence. Monitoring and projecting the deformation within the excavation structure and adjacent formations can offer effective guidance for the seamless advancement of the excavation endeavor. This study aims to prognosticate the deformation originating from foundation pit construction by leveraging the historical time series. Nonetheless, when historical data exhibits high-order nonlinearity and intricate dynamics, the endeavor of forecasting becomes exceedingly formidable.

This paper is dedicated to the precise prediction of forthcoming sequences of deformations (e.g., strain) within the soil mass encompassing the foundation pit, relying on prior records. Specifically, the deformation of the foundation pit's surrounding soil mass often conforms to a monthly trend (reflecting long-term dependency) coupled with

substantial fluctuations. Moreover, notable shifts in strains are improbable on a daily basis; rather, they tend to follow trends over spans of days or weeks (illustrating short-term interdependence). Additionally, the monitoring points pertinent to soil deformation surrounding the foundation pit adhere to specific underlying physical principles. Taking into consideration both the temporal interconnections and spatial associations present within the data, we propose a Multi-Point Recurrent Convolutional Neural Network (RCNN) approach for anticipating the deformation within the foundation pit's adjoining soil mass. This approach adeptly captures both long-term and short-term patterns, thus providing a comprehensive predictive model.

III. MULTI-POINT RCNN FOR SOIL DEFORMATION FORECASTING

This section outlines the framework of the novel Multi-Point Recurrent Convolutional Neural Network (RCNN) proposed for the prediction of soil deformation within the vicinity of foundation pits. This innovative architecture constitutes a harmonious fusion of LSTM and convolutional layers, thereby offering an advanced predictive mechanism [25]. The exposition begins by elucidating the fundamental tenets of the Multi-Point RCNN concept. Subsequently, the depiction of the Multi-Point RCNN network is provided, contextualized within the domain of deformation prediction.

A. RCNN FRAME

The Recurrent Convolution Neural Network (RCNN) amalgamates the feature extraction capabilities inherent in a convolutional neural network (CNN) with the temporal processing proficiencies of a long short-term memory (LSTM), as depicted in Figure 1. The RCNN architecture orchestrates the transformation of input sequences into output sequences in chronological pairs within the temporal realm ($\tau = 1; 2; \ldots; t$). This neural network harnesses CNN layers to draw forth the latent information, i.e., data features, from the input dataset. Subsequently, these data features are channeled to the LSTM layer, wherein the temporal relationships embedded within the time sequence undergo processing facilitated by LSTM's information storage and forgetting mechanisms. Ultimately, a high-level correspondence is established between the model's output and the spatiotemporal attributes of the input data, thereby facilitating the extraction of pertinent insights from the time series. This approach empowers the RCNN architecture to adeptly capture the sequence-to-sequence relationships while encapsulating the temporal dynamics inherent to nonlinear system responses. Furthermore, the CNN layer contributes to the culling of superfluous data, culminating in a mitigation of computational burdens due to its adeptness in abstracting features.

A time series feature chain can be obtained by applying a convolutional layer to the acceleration of ground motion,
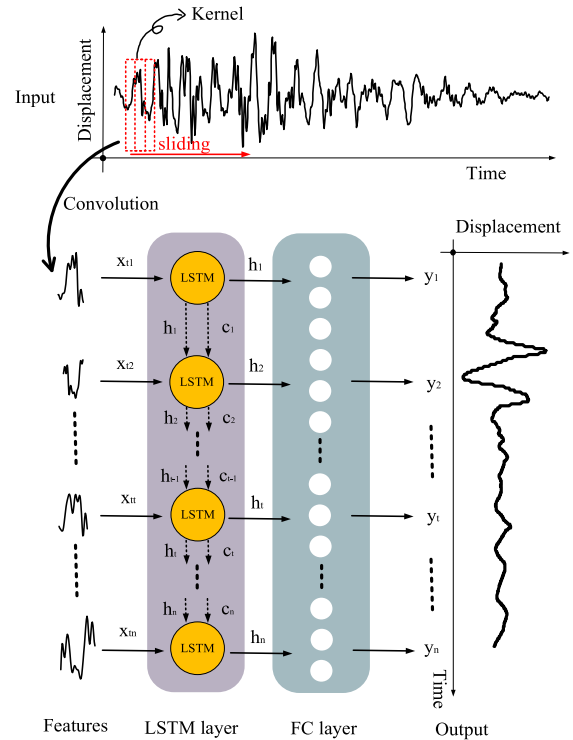

FIGURE 1. Structural diagram of RCNN.

as shown in the following equation:

$$x_t = f(\ddot{x}_g \otimes W + b) \tag{1}$$

The extracted eigenvector is denoted by x_t, while $\ddot{x}_g$ refers to the input data in the form of the acceleration of ground motion. The convolution operation, denoted by $\otimes$, is applied to the input data using a weight parameter W and a bias b, with the activation function $f(\cdot)$ applied afterward. The resulting time-dependent feature chain (Eq. 1) is then fed into the LSTM:

The forgetting gate:

$$f_t = \sigma(x_t W_x^f + h_{t-1} W_h^f) \tag{2}$$

The input gate:

$$i_t = \sigma(x_t W_x^i + h_{t-1} W_h^i) \tag{3}$$

And

$$\tilde{C}_t = tanh(x_t W_x^c + h_{t-1} W_h^c) \tag{4}$$

The output gate:

$$o_t = \sigma(x_t W_x^o + h_{t-1} W_h^o) \tag{5}$$

The memory unit:

$$C_t = \sigma(f_t \times C_{t-1} + i_t \times \tilde{C}_t) \tag{6}$$

The output unit:

$$h_t = tanh(C_t) \times o_t \tag{7}$$

Finally, the target data is connected to the fully connected layer to compute the loss value and perform feedforward.
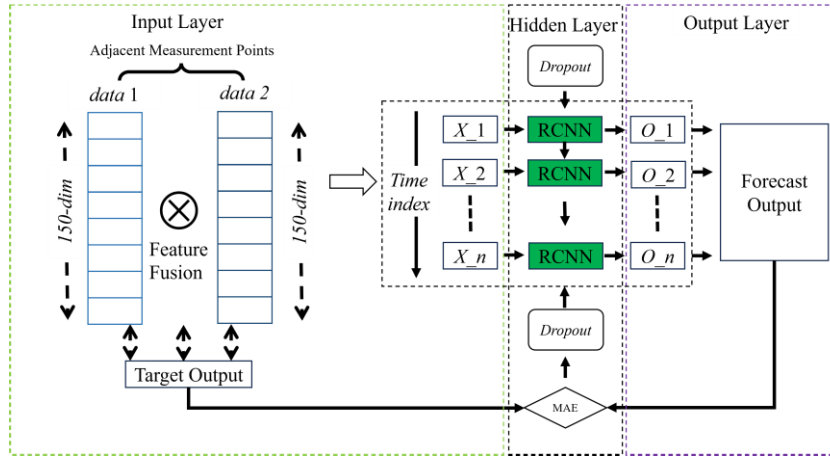
FIGURE 2. Structural diagram of multi-point RCNN.

B. MULTI-POINT RCNN FRAME

This paper introduces an advanced version of the Multi-Point Recurrent Convolution Neural Network (RCNN) sensor temporal prediction model through the integration of data feature fusion. This enhanced model is particularly valuable for capturing intricate correlations existing over extended distances and the multi-point associations within distinct sensor data sets in practical industrial contexts. The architectural layout of the model consists of three layers: the input layer, the hidden layer, and the output layer. The input layer functions as a regulator of the input data's format, whereas the hidden layer constitutes a composite structure housing multiple RCNN units. This facet of the model operates by iteratively adjusting weights until convergence is achieved, thereby diminishing errors. Finally, the output layer restores the outcome to its original data format, as illustrated in Figure 2, which delineates the model's topological configuration.

The approach for augmenting data feature fusion is outlined as follows:

$$X_f = \phi_f \{T_i (X_i)\} \quad i \in c \tag{8}$$

$$X_p' = \phi_p(X_f) \quad p \in P \tag{9}$$

$$loc, class = \phi_{c,l}(\cup X_p') \quad p \in P \tag{10}$$

where T_i means the transformation function of each source feature map before being concatenated together. ϕ_f is the feature fusion function. ϕ_p is the function to generate pyramid features. $\phi_{c,l}$ is the method to predict object from the provided feature maps. *Loc* is localization and *class* is classification.

As observed in Figure 2, the input layer undertakes the task of converting pre-processed sensor time series data into a format conducive for supervised learning, all the while integrating data features from neighboring measurement points. To accomplish this, T time steps are selected as intervals, with the data from the previous T time steps employed as inputs for each time point. Concurrently, the corresponding sample value is assigned as the target output. This array is subsequently directed to the hidden layer, wherein the time step functions as the singular index.

The adaptability to modify the quantity of hidden layers based on data attributes and empirical findings holds paramount importance within deep neural network modeling. Nevertheless, excessive hidden layers can precipitate overfitting, particularly when confronted with data exhibiting pronounced regularity. To circumvent this challenge, this study employs a solitary hidden layer structure. Furthermore, the selection of a suitable threshold activation function $\sigma(\cdot)$ significantly shapes the model's construction. In this context, the Rectified Linear Unit (ReLU) function is chosen owing to its ability to counter gradient diffusion and expedite computation. The output layer employs the Mean Absolute Error (MAE) as the designated loss function to quantify the variance between the projected output and the target output. The gradient calculated from this loss function through reverse propagation adjustment facilitates the fine-tuning of all weights at the hidden layer. The Adam algorithm is harnessed to generate optimization parameters for each learning iteration, persisting until convergence of the loss function is attained. Upon completion of model training, the output layer processes the outcomes, encompassing reverse normalization, to restore the projected value to the format of the input's time series data.

IV. EXPERIMENTAL EXAMPLE

The project encompasses a main museum spanning 6 stories, with a height of 39.00 meters, alongside a public youth education center spanning 2 stories and standing at a height of 12.00 meters. These two components are interconnected as a unified building. Additionally, the entire site has three levels of underground, with a depth of 14.85m and a design elevation of -4.30m for the bottom plate. The standard foundation pit section is executed using the approach of sequential open excavation. Here, an 800-millimeter-thick continuous underground wall serves as the retaining structure. Within this
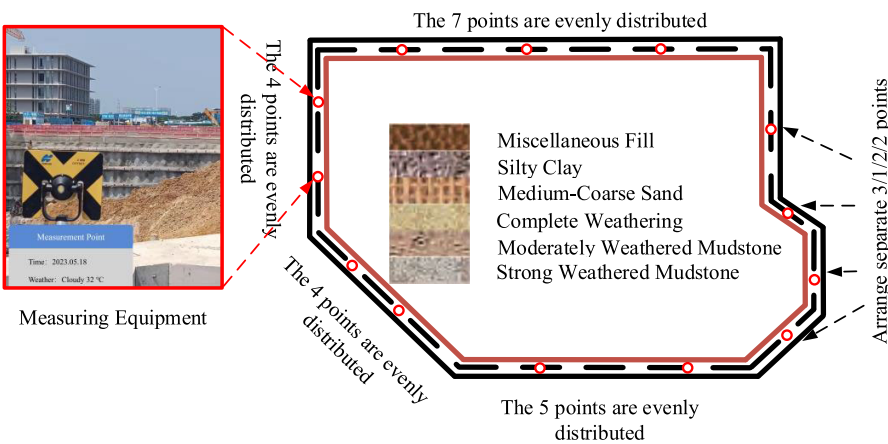
FIGURE 3. Plan of foundation pit and layout of inclinometer tubes.

standard foundation pit segment, a concrete support measuring 0.8 meters by 1 meter is deployed, accompanied by three steel supports. These steel supports possess a diameter of 609 millimeters and a thickness of 16 millimeters. The excavation depth for this standard segment reaches 16.95 meters.

The outcomes of the exploratory efforts consistently reveal a sedimentation pattern at the site. The stratigraphy of the site can be delineated from upper to lower layers. At the surface, a general distribution of road structure layers and miscellaneous fill is evident, spanning a thickness ranging from 1.10 to 3.20 meters. The intermediate section encompasses layers of silty clay and medium-coarse sand. The thickness of silty clay varies from 4.30 to 23.80 meters, while the thickness of medium-coarse sand fluctuates within the range of 0.10 to 1.30 meters. The lowermost layer comprises mudstone, further subcategorized into completely weathered (1.10-4.10 meters), moderately weathered (3.20-22.30 meters), and strongly weathered mudstone (1.60-9.10 meters) strata. Figure 3 visually illustrates the foundation pit layout and inclinometer tube arrangement. Complementing this, Table 1 presents a comprehensive compilation of the geotechnical parameters pertaining to the rock-soil mass. To facilitate the effective monitoring of the wall's horizontal deformation and to ensure the timely adjustment of the support structure during construction, the project has incorporated the use of a YT-610F active vertical inclinometer. A total of 28 points were monitored. These points were evenly distributed along the 8 edges of the foundation pit. Figure 3 illustrates the detailed layout. The monitoring is conducted once a day, and a comprehensive set of 28 data points has been consistently monitored for a continuous duration of 5 months. The collected monitoring data is divided into a training set, a validation set, and a prediction set for implementing the model. Detailed explanations will be presented in the following paragraph.

This section is dedicated to showcasing the effectiveness of our proposed spatiotemporal learning framework, founded upon the Multi-Point RCNN model, in predicting

TABLE 1. Mechanical parameters of soils.

Geomaterials	Consolidated undrained shear force		Static lateral pressure coefficient/K0	Subgrade reaction coefficient	
	c_{cu}/kPa	φ_{cu}/°		KH/(M p/m)	KV/(M p/m)
Silty Clay	27	15	0.42	30	25
Silty Clay	31	16	0.4	30	35
Medium-Fine Sand	0	25	0.38	35	30
Silty Clay	26	14	0.46	15	20
Medium-Coarse Sand	0	31	0.36	28	29
Complete Weathering Mudstone	37	22	0.33	35	40
Moderately Weathered Mudstone	116	31	0.27	200	220
Strong Weathered Mudstone	46	28	0.33	130	160

the deformation monitoring outcomes for an excavation pit. To highlight the advantages of our methodology, we will present its favorable performance across two distinct scenarios characterized by varying time intervals. One scenario involves daily measurements, while the other encompasses weekly measurements, both targeted towards forecasting future strain patterns. Moreover, we intend to underscore the superiority of our approach by conducting a comparative analysis. We will juxtapose the performance of our proposed method against that of the conventional LSTM and RCNN networks, with a particular emphasis on forecasting efficacy. This comparative evaluation aims to firmly establish the enhanced performance of our proposed spatiotemporal learning framework.

The entirety of the measurements recorded between December 5, 2022, and May 18, 2023 (as depicted in Fig. 3),

is initially partitioned into three distinct segments to facilitate training, validation, and testing procedures. Specifically, the training and validation datasets encompass measurements spanning 3 months (from December 2022 to March 2023) and 1 month (April 2023), respectively. Both these datasets serve as the known measurements for training the model. It's essential to emphasize that the training dataset must span a minimum of one month to adequately capture the underlying long-term temporal dependencies that occur on a monthly basis. The remaining measurements spanning one month (May 2023), referred to as the prediction dataset, are treated as unknown measurements. This dataset is employed to evaluate the predictive performance of the trained model. This setup allows for a rigorous assessment of the model's capability to forecast outcomes in scenarios where the data remains unobserved during the training phase. The Multi-Point RCNN, RCNN, and LSTM models, and the details are shown in Table 2.

TABLE 2. Details of deep neural network models.

Models	Multi-Point RCNN	RCNN	LSTM
Epochs	50000	50000	50000
Number of parameters	43,521	39,927	36,961
Number of layers	7	7	6
Filter size	50	50	-
Pooling size	2	2	-
Kernel size	3	3	-
Activation function	ReLu	ReLu	ReLu
Learning rate	0.001	0.001	0.001
Weight decay	0.0001	0.0001	0.0001
The probability of dropout	0.5	0.5	0.5
Number of layers	7	7	7
Number of training data sets	3 months	3 months	3 months
Number of validation data sets	1 months	1 months	1 months
Number of prediction sets	1 months	1 months	1 months

Initially, the recorded data undergo resampling and pre-processing procedures to generate numerous input-to-output samples that conform to the stipulated framework for spatiotemporal analysis. To achieve this, each sample's input must be structured as a 5D array. In this arrangement, the elements are accommodated in the first dimension as batches or samples. Subsequently, the 2nd dimension accounts for the time steps, which can be based on either daily or weekly measurements. The spatial layout of sensors, represented by rows and columns, is encompassed within the 3rd and 4th dimensions. Lastly, the input features, such as displacement values, are housed in the 5th dimension. Likewise, the output for each sample takes on a 3D form. Here, the first dimension corresponds to the samples, followed by the second dimension representing the time steps, and the third dimension encapsulating the output features. These output features could encompass, for instance, the strain responses of individual sensors.

Both the input and output data are channeled into the envisaged Multi-Point RCNN network, as illustrated in Figure 2, to facilitate model training. Given the substantial volume of training data entailing significant memory requirements, a batch size of 50 is chosen. This indicates that 50 samples from the training dataset are employed to assess the gradient of the loss function and subsequently update the learnable parameters—such as network weights and biases. For initializing these parameters, the weights pertaining to the Multi-Point RCNN and Fully Connected (FC) layers are endowed with random initialization via the glorot uniform initializer [26]. Correspondingly, the biases are set to initiate at zero.

The training phase encompasses a span of 5000 epochs, dedicated to acquiring an understanding of the temporal and spatial interdependencies inherent in the dataset. In a bid to optimize training efficiency, all data is rescaled to the range of $[-1, 1]$ through employment of the MinMaxScaler available in the scikit-learn toolkit. Additionally, the training data is subjected to shuffling before the initiation of each epoch. This shuffling practice serves a twofold purpose: mitigating model variance and expediting the convergence process [27]. Throughout the training iteration, the model undergoes validation utilizing the validation dataset post completion of each epoch, with close monitoring of the validation error. The algorithm is applied to iteratively update weights and biases through the process of backpropagation, aiming to systematically minimize the objective function. It's important to emphasize that the model is conditioned using the validation dataset. As the training process progresses, both the training and validation errors exhibit a consistent decrease, particularly during the early stages of training. This pattern demonstrates the effectiveness of our approach in generating extremely low training and validation loss values across all scenarios, indicative of exceptional training efficacy.

To demonstrate the strong robustness of the Multi-Point RCNN model, we selected Y1 and Y2 monitoring points on different sides of the foundation pit. In the initial context, the model is employed to predict daily strain oscillations relying on historical monthly data as input. Fig. 4 (a) displays the predicted daily strain responses for sensor Y1, employing historical daily data as input. The results demonstrate the model's proficiency in capturing the extended temporal patterns of strain responses. Upon closer examination, the zoomed-in view underscores that the predicted strain responses align closely with the actual field measurements, underscoring the model's precision in anticipating short-term oscillations. In the subsequent scenario, our investigation delves into the prediction of daily strain responses grounded on an extended span of input measurements. Fig. 4 (b) exhibits the predicted daily strain responses for sensor Y2. Significantly, the strain responses are precisely anticipated in regards to both amplitudes and phases. In contrast to
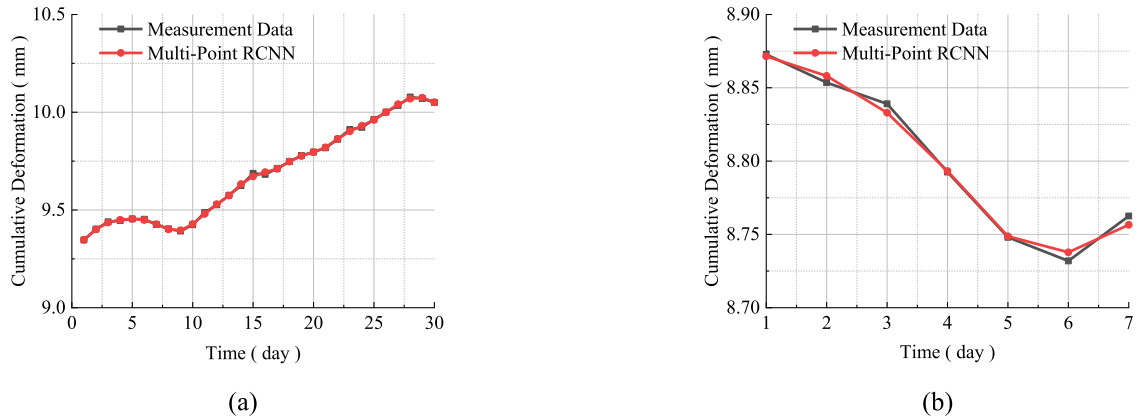
FIGURE 4. The prediction results of the multi point RCNN model in long and short periods.
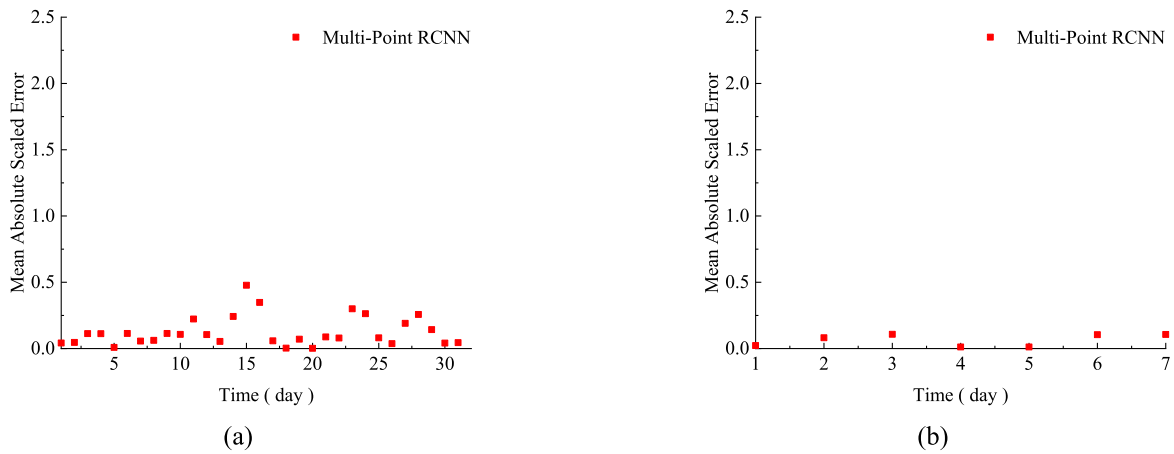

FIGURE 5. The MASE of the multi point RCNN model in long and short periods.

the initial scenario, it becomes evident that utilizing an extended span of measurements as input augments prognostic efficacy, particularly with regards to peak outcomes. Nevertheless, despite employing daily measurements as input, our approach proficiently anticipates forthcoming outcomes with remarkable precision. This vividly underscores the robust spatiotemporal feature learning capabilities inherent in the proposed Multi-Point RCNN method.

For enhanced visualization of the prediction error, the Mean Absolute Scaled Error (MASE), encapsulating the normalized error distribution as defined in Equation (11), is depicted for all sensors in Fig. 5. The graph discernibly exhibits consistent errors for both long-term and short-term predictions. This observation substantiates the assertion that the proposed Multi-Point RCNN method boasts substantial robustness.

$$\text{MASE} = \left| \frac{\hat{\varepsilon}_{i,t}^2}{\frac{1}{T}\sum_{t=2}^{T}|y_t - y_{t-1}|} \right| \qquad (11)$$

A comparison between our proposed approach, the conventional LSTM, and RCNN has been carried out employing

identical training, validation, and prediction datasets. In the RCNN methodology, both input and output are organized as 3D arrays. In this configuration, the 1st dimension indicates samples, the 2nd dimension signifies time steps, and the 3rd dimension encapsulates input or output features. Since the RCNN does not explicitly address spatial associations, the sensor count is considered tantamount to the number of features. Figure 6 showcases the anticipated strain responses within the RCNN framework, utilizing historical daily measurements as input. While the model successfully predicts long-term trends, it encounters challenges when it comes to accurately forecasting short-term oscillations. Furthermore, a comparison is conducted involving response forecasting through the traditional LSTM network. Both training and validation datasets, encompassing records from all sensors, are employed for this purpose. Fig. 6 portrays the one-step-ahead predicted strain responses for sensors, grounded in past daily measurements. Similar to the RCNN outcomes, the LSTM predictions demonstrate an ability to capture the overarching daily trends, yet they struggle to accurately encapsulate the immediate strain fluctuations. Furthermore, the training
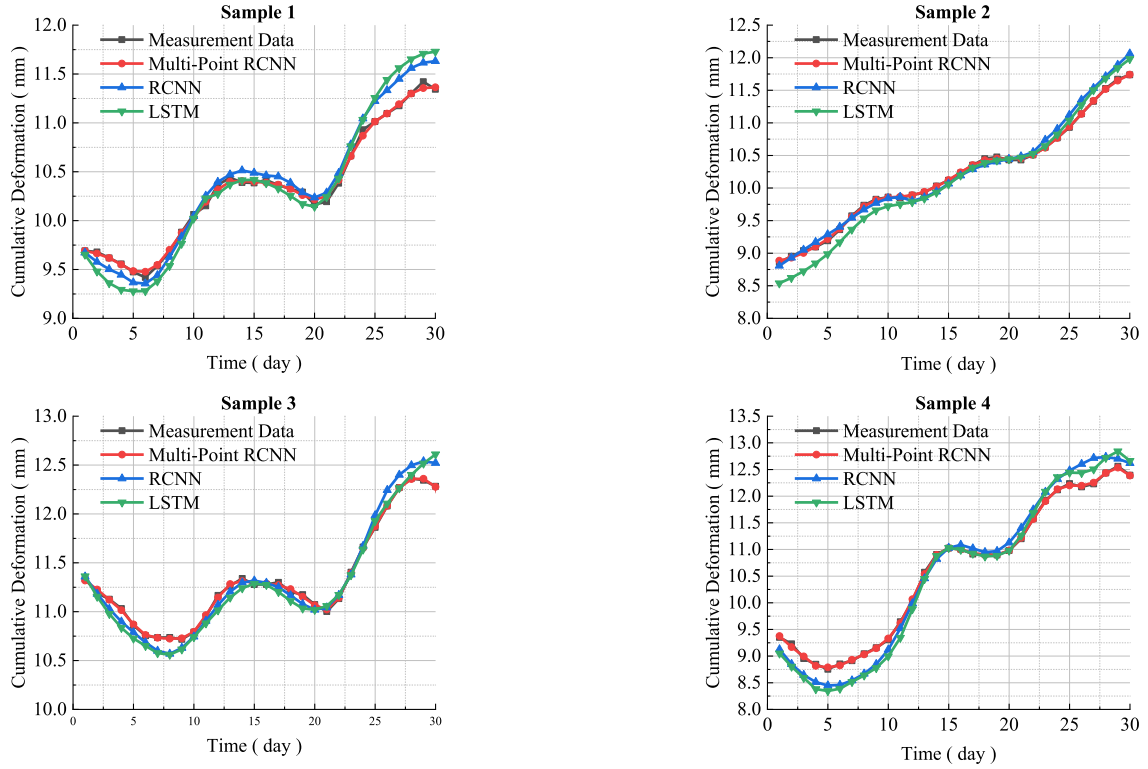
FIGURE 6. Comparison of three types of models for prediction.
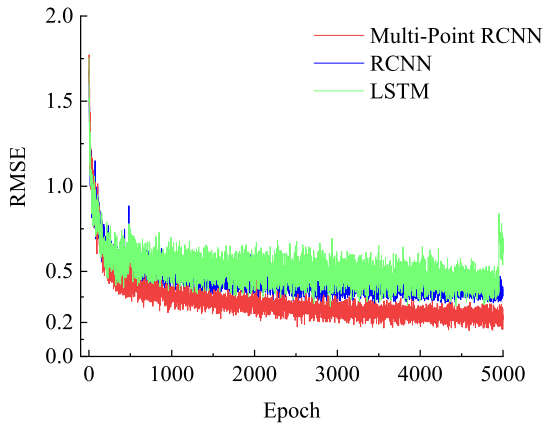

FIGURE 7. The training loss of three types of models for prediction.

loss, as depicted in Fig. 7, underscores the superiority of our proposed model's training process. This figure elucidates the notable advantage of our approach in terms of training efficacy.

To provide a clearer depiction of the prediction error, the Probability Density Function (PDF) of the normalized error distribution, as defined in Equation (12), is employed. The analysis reveals that the prediction errors generated by the Multi-Point RCNN are predominantly concentrated within the range of 10% for all sensors, with a high confidence

interval (CI) of 96%. In contrast, the RCNN achieves a CI of 82%, and the LSTM network exhibits a CI of 79%, as showcased in Figure 8. This discernible pattern unequivocally highlights the substantial superiority of the Multi-Point RCNN approach over both RCNN and LSTM, particularly in forecasting responses characterized by robust spatiotemporal dependencies.

$$\pi_i = \mathrm{PDF} \left\{ \frac{y_i^{\mathrm{ture}} - y_i^{\mathrm{pred}}}{\max \left(\left| y_i^{\mathrm{ture}} \right| \right)} \right\} \tag{12}$$

Concurrently, an analysis of the Mean Absolute Scaled Error (MASE) was undertaken. The distribution of MASE results, as depicted in Figure 9, reveals noteworthy insights. The Multi-Point RCNN model, as proposed within this paper, demonstrates a consistent and uniform distribution of prediction errors across the entirety of its performance, underscoring the model's robustness. In contrast, both the RCNN and traditional LSTM models exhibit less uniform distribution of prediction errors, with the traditional LSTM model displaying particularly uneven error distribution.

Concurrently, an analysis of the Error Rate was performed. The Error Rate is defined as the ratio of the absolute value of the maximum error in the predicted result to the maximum measured value. As shown in Figure 10, it becomes evident that the Multi-Point RCNN model proposed in this article
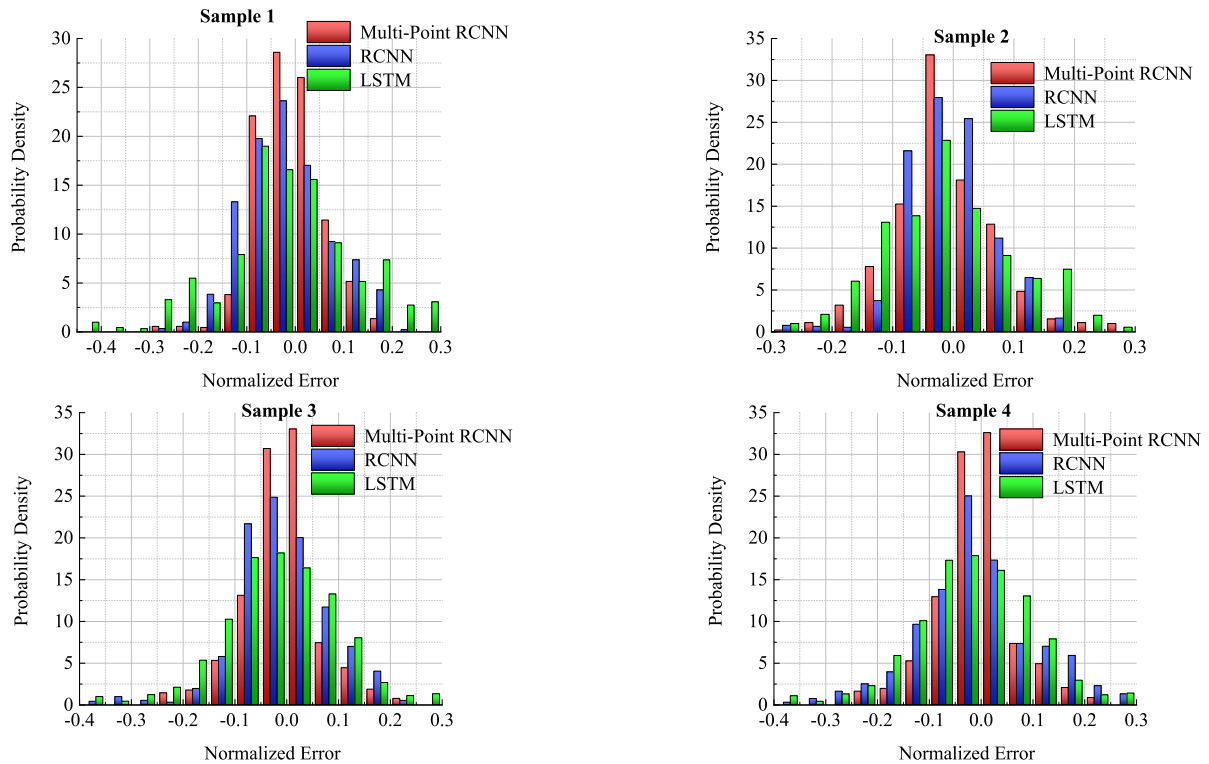
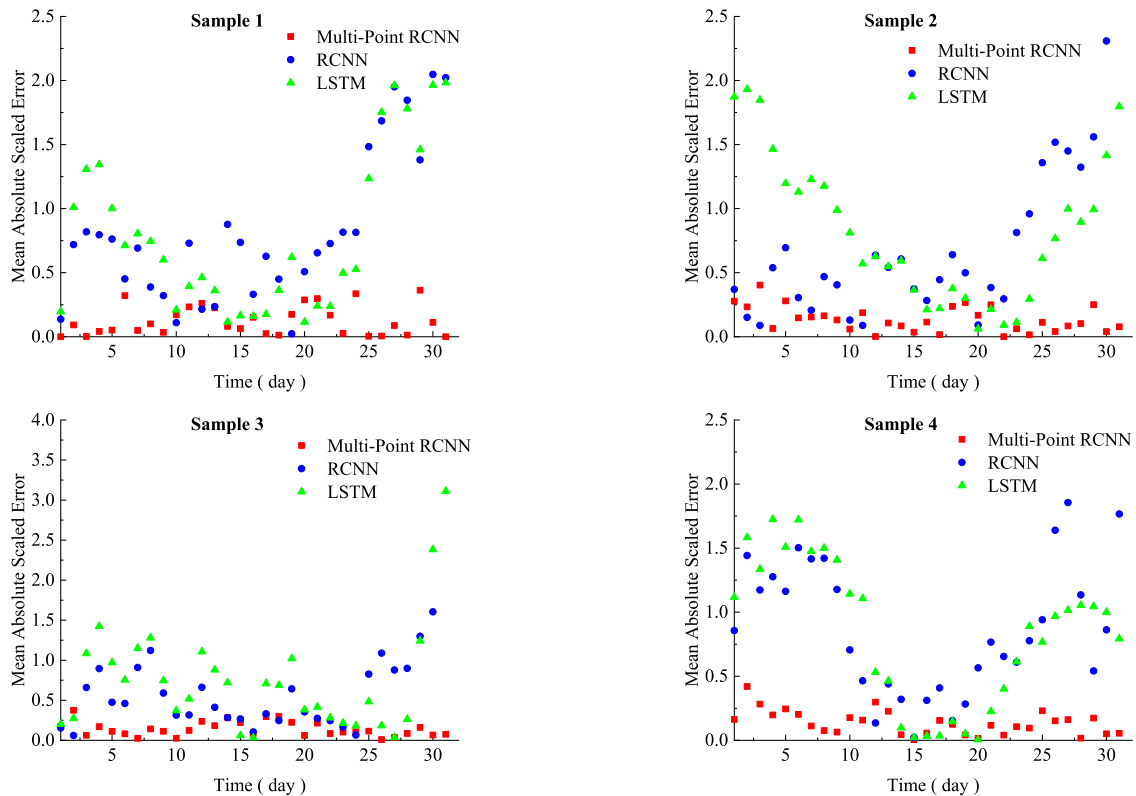**FIGURE 8.** The PDF of three types of models for prediction.

FIGURE 9. The PDF of three types of models for prediction.

exhibits notable advantages in terms of absolute prediction accuracy. The Table 3 highlights that the Multi-Point RCNN

model exhibits the smallest error rate compared to the other models. Sample 3 demonstrates a maximum prediction error
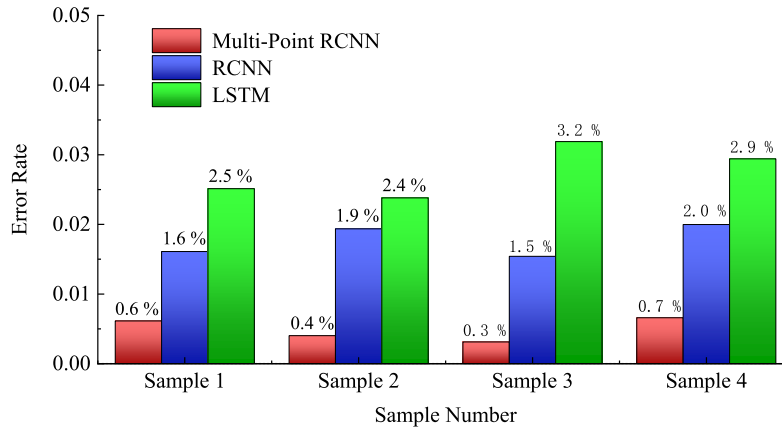
FIGURE 10. The error rate of three types of models for prediction.

TABLE 3. Predictive performance of three models.

Model	CI of error 10 %	R^2	Error rate of sample 1	Error rate of sample 2	Error rate of sample 3	Error rate of sample 4
Multi-Point RCNN	96%	0.966	0.6%	0.4%	0.3%	0.7%
RCNN	82%	0.877	1.6%	1.9%	1.5%	2.0%
LSTM	79%	0.801	2.5%	2.4%	3.2%	2.9%

of merely 0.3%, which is 5 times lower than that of the RCNN model (1.5%) and almost 11 times lower than the LSTM model (3.2%).

V. CONCLUSION

This paper presents an innovative spatiotemporal learning framework founded on the Multi-Point RCNN. This approach is designed to forecast the deformation arising from foundation pit excavation, effectively capturing both spatial associations and long short-term temporal interconnections. The proposed spatiotemporal deep learning approach encompasses a Multi-Point RCNN layer, facilitated by data feature fusion, and finally a Fully Connected layers, all of which collectively model the intricate spatiotemporal interdependencies within the input-to-output samples. Central to this approach is the utilization of the Multi-Point RCNN layer, which adeptly learns spatiotemporal characteristics from the field sensing measurements. To substantiate its effectiveness, the presented methodology is employed for forecasting deformation in foundation pits, leveraging a dataset encompassing strain time-history measurements spanning a period of five months. Comparative analyses are conducted against both the RCNN model and the traditional LSTM network, which lack the capacity to adequately model such intricate spatiotemporal dependencies. The analysis reveals that the prediction errors generated by the Multi-Point RCNN are predominantly concentrated within the range of 10% for all sensors, with a high-confidence interval (CI) of 96%, compared to the RCNN model (82%) and the LSTM model (79%). It is particularly noteworthy that Sample 3 demonstrates a maximum

prediction error of merely 0.3%, which is 5 times lower than that of the RCNN model (1.5%) and almost 11 times lower than the LSTM model (3.2%).

The results unequivocally demonstrate the potency of the proposed Multi-Point RCNN model in the realm of long short-term response prognosticating. Moreover, they emphasize the inadequacy of depending exclusively on temporal features without explicitly encoding spatial correlations to achieve precise response prediction. It is noteworthy that the trained Multi-Point RCNN model exhibits commendable computational efficiency, enabling real-time prediction. This feature extends its potential applicability to other areas, including fault detection. However, it is acknowledged that a constraint of the proposed methodology lies in its reliance on sensors positioned within Euclidean grids. In scenarios entailing non-uniform sensor configurations, the investigation of geometric or graph-theoretic modeling shows potential and is expected to constitute a central aspect of our forthcoming research undertakings.

REFERENCES

[1] C. Zhu, Z. Yan, Y. Lin, F. Xiong, and Z. Tao, "Design and application of a monitoring system for a deep railway foundation pit project," *IEEE Access*, vol. 7, pp. 107591–107601, 2019.

[2] Y.-X. Wu, H.-M. Lyu, J. Han, and S.-L. Shen, "Dewatering-induced building settlement around a deep excavation in soft deposit in Tianjin, China," *J. Geotech. Geoenviron. Eng.*, vol. 145, no. 5, May 2019, Art. no. 05019003.

[3] C.-F. Zeng, G. Zheng, X.-F. Zhou, X.-L. Xue, and H.-Z. Zhou, "Behaviours of wall and soil during pre-excavation dewatering under different foundation pit widths," *Comput. Geotechnics*, vol. 115, Nov. 2019, Art. no. 103169.

[4] T. Yang, S. Liu, X. Wang, H. Zhao, Y. Liu, and Y. Li, "Analysis of the deformation law of deep and large foundation pits in soft soil areas," *Frontiers Earth Sci.*, vol. 10, Feb. 2022, Art. no. 828354.

[5] Y. Tan and D. Wang, "Characteristics of a large-scale deep foundation pit excavated by the central-island technique in Shanghai soft clay. I: Bottom-up construction of the central cylindrical shaft," *J. Geotech. Geoenviron. Eng.*, vol. 139, no. 11, pp. 1875–1893, Nov. 2013.

[6] S. Wang, Q. Li, J. Dong, J. Wang, and M. Wang, "Comparative investigation on deformation monitoring and numerical simulation of the deepest excavation in Beijing," *Bull. Eng. Geol. Environ.*, vol. 80, no. 2, pp. 1233–1247, Feb. 2021.

[7] Y. Sun and H. Xiao, "Wall displacement and ground-surface settlement caused by pit-in-pit foundation pit in soft clays," *KSCE J. Civil Eng.*, vol. 25, no. 4, pp. 1262–1275, Apr. 2021.

[8] J. Cui, Z. Yang, and R. Azzam, "Field measurement and numerical study on the effects of under-excavation and over-excavation on ultra-deep foundation pit in coastal area," *J. Mar. Sci. Eng.*, vol. 11, no. 1, p. 219, Jan. 2023.

[9] J. Chen, Q. Xu, X. Luo, A. Tian, S. Xu, and Q. Tang, "Safety evaluation and energy consumption analysis of deep foundation pit excavation through numerical simulation and in-site monitoring," *Energies*, vol. 15, no. 19, p. 7099, Sep. 2022.

[10] M.-G. Li, X. Xiao, J.-H. Wang, and J.-J. Chen, "Numerical study on responses of an existing metro line to staged deep excavations," *Tunnelling Underground Space Technol.*, vol. 85, pp. 268–281, Mar. 2019.

[11] Y. Yang, J. Li, C. Liu, J. Ma, S. Zheng, and W. Chen, "Influence of deep excavation on adjacent bridge piles considering underlying Karst cavern: A case history and numerical investigation," *Acta Geotechnica*, vol. 17, no. 2, pp. 545–562, Feb. 2022.

[12] H. Liu, K. Li, J. Wang, and C. Cheng, "Numerical simulation of deep foundation pit construction under complex site conditions," *Adv. Civil Eng.*, vol. 2021, Feb. 2021, Art. no. 6669466.

[13] R. Zhang, Z. Chen, S. Chen, J. Zheng, O. Büyüköztürk, and H. Sun, "Deep long short-term memory networks for nonlinear structural seismic response prediction," *Comput. Struct.*, vol. 220, pp. 55–68, Aug. 2019.

[14] F.-C. Chen and M. R. Jahanshahi, "NB-CNN: Deep learning-based crack detection using convolutional neural network and Naïve Bayes data fusion," *IEEE Trans. Ind. Electron.*, vol. 65, no. 5, pp. 4392–4400, May 2018.

[15] B. K. Oh, Y. Park, and H. S. Park, "Seismic response prediction method for building structures using convolutional neural network," *Struct. Control Health Monitor.*, vol. 27, no. 5, May 2020, Art. no. e2519.

[16] T. Kim, O.-S. Kwon, and J. Song, "Response prediction of nonlinear hysteretic systems by deep neural networks," *Neural Netw.*, vol. 111, pp. 1–10, Mar. 2019.

[17] Z. Xing, S. Zhao, W. Guo, F. Meng, X. Guo, S. Wang, and H. He, "Coal resources under carbon peak: Segmentation of massive laser point clouds for coal mining in underground dusty environments using integrated graph deep learning model," *Energy*, vol. 285, Dec. 2023, Art. no. 128771.

[18] Y. Wu, S. Zhao, Z. Xing, Z. Wei, Y. Li, and Y. Li, "Detection of foreign objects intrusion into transmission lines using diverse generation model," *IEEE Trans. Power Del.*, vol. 38, no. 5, pp. 3551–3560, Oct. 2023.

[19] S. Hochreiter and J. Schmidhuber, "Long short-term memory," *Neural Comput.*, vol. 9, no. 8, pp. 1735–1780, Nov. 1997.

[20] I. Sutskever, O. Vinyals, and Q. V. Le, "Sequence to sequence learning with neural networks," in *Proc. Adv. Neural Inf. Process. Syst.*, vol. 27, 2014, pp. 3104–3112.

[21] P. Xie, A. Zhou, and B. Chai, "The application of long short-term memory (LSTM) method on displacement prediction of multifactor-induced landslides," *IEEE Access*, vol. 7, pp. 54305–54311, 2019.

[22] P. Zhang, H.-N. Wu, R.-P. Chen, T. Dai, F.-Y. Meng, and H.-B. Wang, "A critical evaluation of machine learning and deep learning in shield-ground interaction prediction," *Tunnelling Underground Space Technol.*, vol. 106, Dec. 2020, Art. no. 103593.

[23] Q. Jiangu, W. Anhai, and J. Jun, "Nonlinear time series prediction of geotechnical engineering based on wavelet optimization LSTM-ARMA model," *J. Tongji Univ., Nat. Sci.*, vol. 49, no. 8, pp. 1107–1115, 2021.

[24] Z. Huajing, Z. Mingyang, and L. Wei, "Dynamic prediction of deformation of ground connected wall in deep foundation pit based on neural network algorithm," *Chin. J. Underground Space Eng.*, vol. 17, no. 1, pp. 321–327, 2021.

[25] Z. Longji, W. Heisha, and Z. Shuang, "Theoretical and experimental study of floating foundation vibration reduction system based on deep neural network," *IEEE Access*, vol. 9, pp. 86107–86118, 2021.

[26] X. Glorot and Y. Bengio, "Understanding the difficulty of training deep feedforward neural networks," in *Proc. 13th Int. Conf. Artif. Intell. Statist.*, vol. 9. Sardinia, Italy: Society for Artificial Intelligence and Statistics, 2010, pp. 249–256.

[27] Q. Meng, W. Chen, Y. Wang, Z.-M. Ma, and T.-Y. Liu, "Convergence analysis of distributed stochastic gradient descent with shuffling," 2017, *arXiv:1709.10432*.

FEI SONG was born in Henan, China. He is currently a Structural Engineer with Huanan Construction Company Ltd., China Construction Sixth Bureau. His current research interests include architectural structural design and deformation control of deep excavation pits.

HUIWU ZHONG was born in Guangdong, China. He is currently a Structural Engineer with Guangdong Shengxiang Traffic Engineering Testing Company Ltd. His current research interests include architectural structural design and deformation control of deep excavation pits.

JIAQING LI was born in Guangdong, China. He received the master's degree from the School of Civil Engineering, Guangzhou University, in 2015, under the supervision of Academician Zhou Fulin. His current research interests include structural vibration displacement analysis, motion control technology, inspection, testing, and monitoring of structures.

HUAYONG ZHANG was born in Guizhou, China. He is currently the Chief Engineer with Huanan Construction Company Ltd., China Construction Sixth Bureau. His current research interest includes the deformation control of deep excavation pits.